DISTRIBUTION STATEMENT A: Approved for public release; distribution is unlimited.

New River Inlet DRI: Observations and modeling of flow and material exchange & Field and Numerical Study of the Columbia River Mouth

Jamie MacMahan & Ad Reniers
Oceanography Department, Spanagel 327c, Naval Postgraduate School, Monterey, CA 93943
Phone: (831) 656-2379 Fax: (831) 656-2712 Email: jhmacmah@nps.edu

NPS Award Number: (N0001411WX20962; N0001412WX20498)
Rosenstiel School of Marine and Atmospheric Science, Miami, FL33149
Phone: (305) 421-4223 Fax: (305) 421-4701 Email: areniers@rsmas.miami.edu
UM Award Number: (N000141010409, N000141010379)

LONG-TERM GOALS

The goal of our effort is to understand river and inlet fluid dynamics through in situ field observations and numerical modeling.

OBJECTIVES

The main objectives of our FY14 effort were to:

- analyze the GPS-equipped drifters, in situ sensors from the NPS mini-catamarans and the USGS tripods from the Mouth of the Columbia River (MCR);
- continue analysis of New River Inlet (NRI) water characterization;
- describe and model the tidal exchange at (NRI) using Delft3D;
- verify Delft3D in predicting the complex velocity field and concurrent sediment transports under a range of environmental conditions (i.e. waves, wind and stratification)

APPROACH

Our approach is to collect field observations to evaluate the sensitivity of Delft3D at the Mouth of the Columbia River and at New River Inlet, NC.

WORK COMPLETED

We (MacMahan, Reniers, Gelfenbaum, students (Patrick Rynne, Micah Weltmer, Jeannette Sheets, and Kyle Baden) and technicians (Andrew Stevens)) have analyzed the various field observations at the MCR in May-June 2013 (RIVET-II) and at NRI in May-June 2012 (RIVET I). Numerical model validation using the in situ field observations is ongoing. We are actively collaborating with PIs involved with RIVET-I and RIVET-II efforts. A number of unique findings are described below.

RESULTS

Salinity, temperature, and CDOM characterization for a tidally chocked estuary connected to two contrasting intra-coastal waterways

The optical properties of water, the wavelengths at which it absorbs and fluoresces, are a function of turbidity and biological content, such as the quantity of phytoplankton or dissolved organic material (DOM) (Smart, 2004). An important fraction of DOM is chromophoric, or color dissolved organic matter (CDOM) that consists of the humic and fluvic acids (yellow substance) of decaying plant matter (Nieke et al., 1997). Like chlorophyll, CDOM is a major light-absorbing constituent in water. CDOM absorption is strongest in the ultraviolet to blue spectrum and decreases exponentially with increasing wavelength (Stedmon, 2000). CDOM affects the quality and quantity of light that reaches photosynthetic cells, thereby controlling phytoplankton production, and hence chlorophyll *a* concentration. As a result, light absorption in coastal waters is dominated by CDOM, while light absorption in ocean waters is dominated by phytoplankton (Nieke, 1997). CDOM has also been found to be conservative in coastal waters (Hojerslev, 1988; Bowers et al., 2000); it is therefore a better optical tracer than chlorophyll.

Bowers et al. (2004, 2008) correlated surface salinity (S) with surface CDOM, owing to its strong optical signature, as method for remotely sensing CDOM to describe the spatial pattern of S. They found a statistically significant negative correlation between S and CDOM resulting in high CDOM corresponding with low salinity values. Bowers and Brett (2008) analytically evaluated the CDOM-S relationship with respect to the ratio of the flushing time to the time scale of the source. The CDOM-S relationship is evaluated longitudinally for New River Inlet (NRI) along the main channel into the backbay (Figure 1a). The CDOM is negatively correlated (R^2=0.71) with S, consistent with Bowers and Brett (2008). Based on the analysis by Bowers and Bret (2008), the linear relationship implies there is a short flushing time along the main channel. However, when including data points for all locations, there is no correlation (R^2=0) between CDOM and S (Figure 1b). This is related to the fact that water in the ICWS is hyper saline with high CDOM, where farther up the estuary the high CDOM is coincident with brackish salinity. Though temperature is not considered a conservative property, there is a crude linear (R^2=0.5) relationship between CDOM and T (Figure 1c).

Though a qualitative interpretation for the identification of the number of "independent" water masses can be ascertained using the spatial maps of T, S, and CDOM, a quantitative measure is preferred. A k-means cluster analysis is performed to partition the T, S, and CDOM data into independent groups. K-means method minimizes the normalized Euclidean distance using random starting positions and a priori defined number of groups. The numbers of groups were determined by performing the K-means method for various size groups. The number of groups was selected based when the sum of distance asymptotes, which is for this dataset result in four groups.

Owing to the randomization of the Euclidean starting location, the classification grouping varied. Therefore, a Monte Carlo simulation was performed to account for the statistical differences of the clustering. All possible outcomes are included, as shown in Figure 2. Solid colors represent 100% association with one group, where partial bins represent that this data point can be associated with more than one group (Figure 2). The fours groups are related to the 1) brackish, warm, high CDOM estuarine water, 2) saline, cold, low CDOM ocean water, 3) hyper saline, warm, high CDOM water, and 4) mixed water. The mixed water is associated with circles with two colors. The results performing the cluster analysis using only T-S (not shown) and using T-S-CDOM are similar, though the partitioning of the mixed water has different binned percentages.

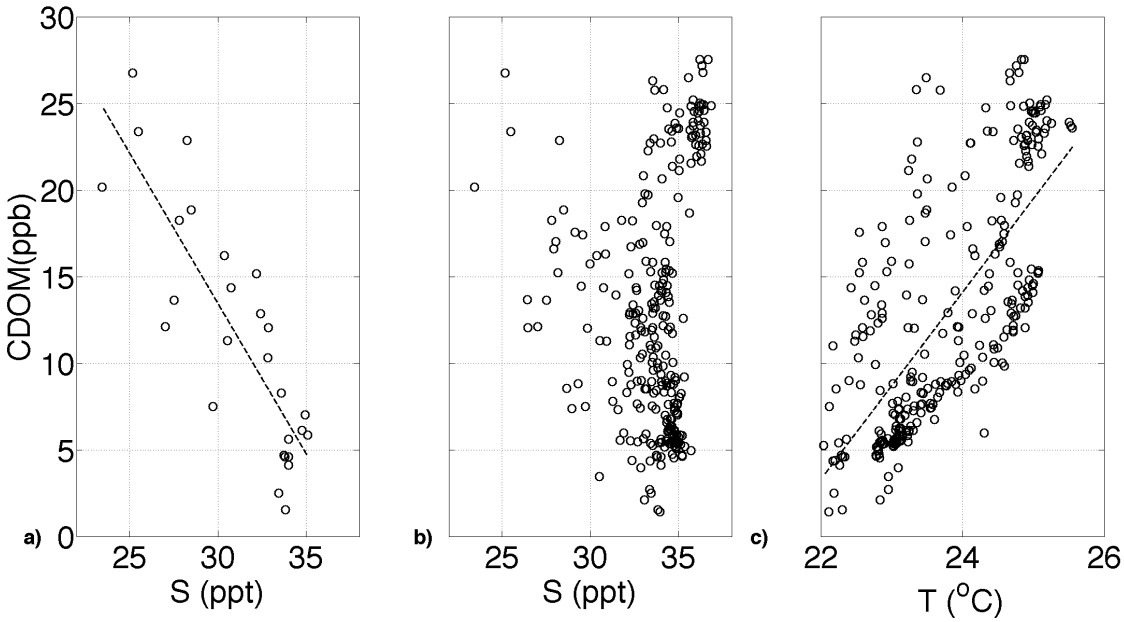

Figure 1. a) CDOM and S relationship for observation along the longitudinal axis of the estuary. **b)** CDOM and S relationship for all observations. **c)** CDOM and T relationship for all observations. Black dashed line represent best-fit linear line.

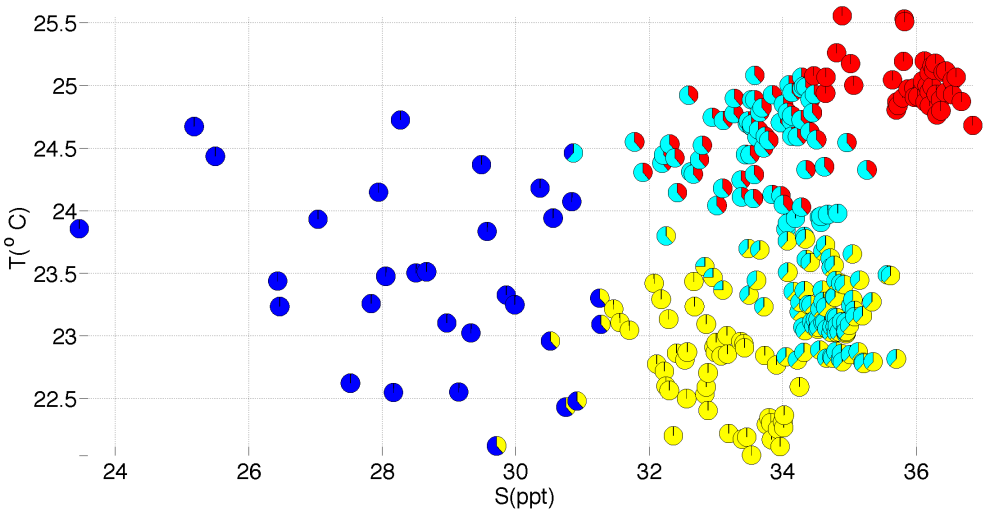

Figure 2. Monte Carlo K-means cluster analysis for T-S-CDOM at NRI. Circles represent T-S observations, colors represent four different classifications, and pie shape represents percentage of occurrence.

Tidal exchange at New River Inlet

On each tidal cycle, a volume of water enters and exits an estuary through the inlet mouth. It is well known that a percentage of this volume is renewed with new seawater on each cycle, a concept that was first introduced by Stommel and Farmer (1952) and widely implemented in the literature (Fischer *et al.,* 1979; Mehta and Joshi, 1988; Signell and Butman, 1992; Chadwick and Largier, 1999). This approach defines the fraction of the tidal prism that leaves an estuary during an ebb tide and does not return on the following flood. This process, often termed 'tidal pumping' drives the transport of

inland water to the sea in estuaries with weak river discharges. In an effort to examine the relationship between tidal exchange and residence time in NRI, a new definition of tidal exchange was developed.

NRI has a complex inlet channel that is surrounded by marshland and connects to both a relatively large backbay and Intracoastal Waterway. This geometry causes irregular tidal flows that can lead to increased exchange. Specifically, the geometry of the inlet can strongly control how much of the tidal prism that enters the inlet on a flood will stay during the following ebb. To account for this, tidal exchange is decomposed into two fractions, an *ocean exchange fraction* and an *estuary exchange fraction*. The ocean exchange fraction is defined as the fraction of ebbing water that leaves the system through the inlet mouth and does not return on the following flood as described in the Stommel and Farmer model. The estuary exchange fraction represents the percentage of flooding water that enters the system through the inlet mouth and stays during the following ebb. The combination of these two fractions controls tidal exchange.

To better understand how these fractions influence tidal exchange and the residence time of water in an estuary like NRI, a series of modeling studies were conducted using a simple tidal prism model and Delft3D. The simple transport model is based on three fundamental assumptions: 1) A fraction of water that leaves an inlet system during an ebb will stay in the sea on the following flood, 2) a fraction of water that enters the inlet on a flood will stay within the estuary on the following ebb, and 3) the remaining water inside the estuary mixes uniformly.

The transport model is compared to the approach by Stommel and Farmer and Delft3D for a variety of inlet geometries. For inlet geometries with low estuary exchange fractions (Figure 3), the Stommel & Farmer approach will over-predict tidal exchange and the transport of estuary water to the sea. This equates to under-predicting the residence time (Figure 4). These findings suggest that to adequately characterize a tidal inlet such as NRI, both exchange fractions should be considered.

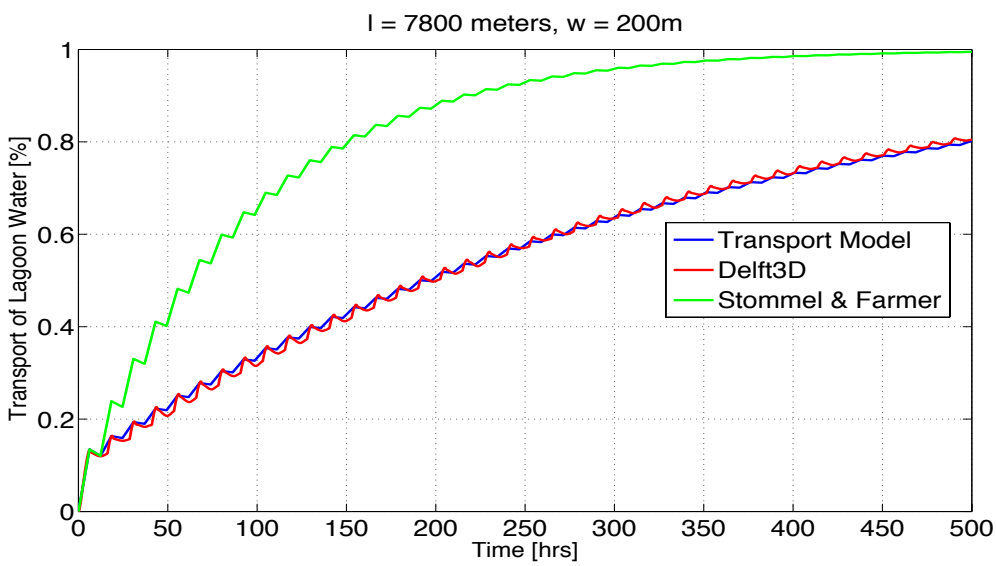

Figure 3. The transport of estuary water out of an idealized inlet with a channel length of 7800 m and channel width of 200 m as predicted by the Stommel and Farmer tidal prism model that includes the ocean exchange fraction but neglects the estuary exchange fraction (green line), a tidal prism model that includes both exchange fraction (blue line), and depth-averaged model in Delft3D (red line).

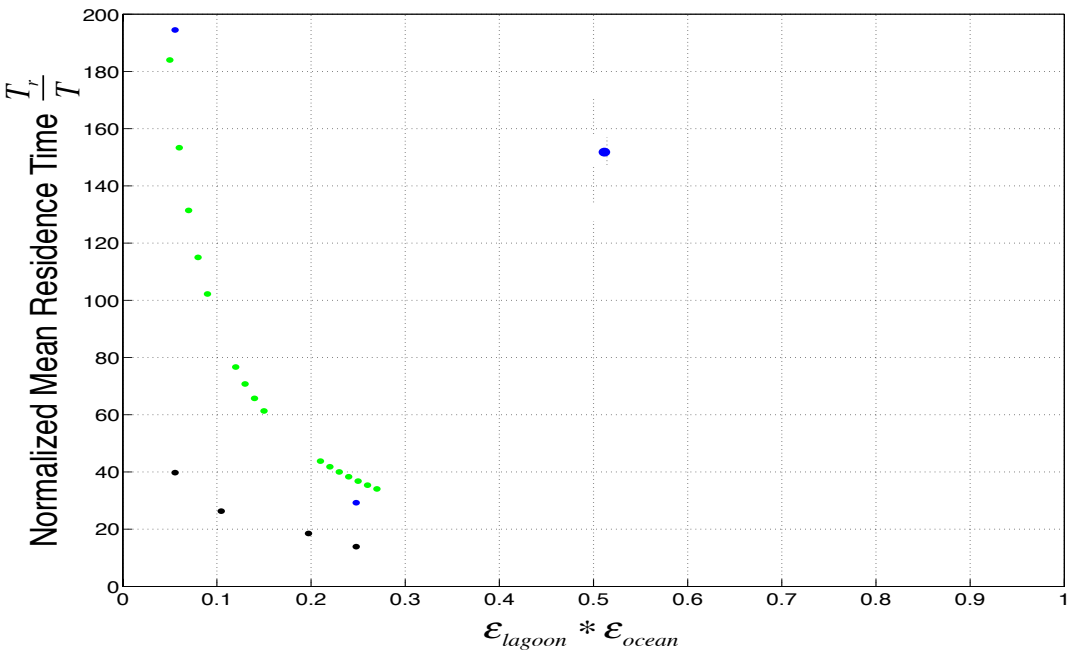

Figure 4. The relationship between the product of the tidal exchange fractions and the mean residence time in a simple basin for 11 inlet geometries using a tidal prism model that includes both exchange fractions (green line), a virtual tracer method in Delft3D (blue line) and the Stommel and Farmer tidal prism model that neglects the estuary exchange fraction.

Wind stress measurements at New River Inlet (in collaboration with Dave Ortiz-Suslow, Brian Haus, Nathan Laxague and Hans Graber)

Observations made at the NRI in North Carolina, during the Riverine and Estuarine Transport experiment (RIVET), are used to evaluate the viability of wind speed dependent, wind stress parameterizations in relatively shallow water. As part of the field campaign, a small, agile research vessel was deployed to obtain high-resolution wind velocity measurements in and around the tidal inlet. The eddy covariance method is used to recover direct estimates of the 10 m natural atmospheric drag coefficient from the three dimensional winds. Observations of wind stress angle, near-surface currents, and heat flux are used to analyze the across-shore variability of wind stress steering off of the mean wind azimuth. In general, for on-shore winds above 5 m/s, the drag coefficient is observed to be two and a half times the predicted open ocean value. Significant wind stress steering is observed within 2 km of the inlet mouth, which is directly proportional to the near-surface current shear. It is determined that outside the influence of typical coastal processes (e.g. land-air atmospheric affects, strong current gradients, wave shoaling, and depth-limited wave breaking) the open ocean parameterizations generally represent the wind stress field.

The Influence of Baker Bay and Sand Island on Circulations in the Mouth of the Columbia River

Lagrangian GPS measurements of position and surface velocity and Eulerian measurements of vertical velocity structure, temperature and salinity were used to study circulation patterns in the mouth of the Columbia River, paying particular attention to the influence of Baker Bay and the Sand Island pile dikes (Figure 5). Tidal range and river discharge are the key drivers in the dynamic lower Columbia River, and the presence of Baker Bay, a shallow sub-embayment, adds further complexity. Drifter surface velocities were greatest during maximum ebb flows and were greater in the South Channel, which is dominated by river discharge, than the North Channel, which is more heavily

influenced by tidal oscillations. Drifters occasionally entered Baker Bay during flood flows via the inlet between West and East Sand Islands, especially in conjunction with strong southwesterly winds. During ebb flows, some drifters were trapped in the Sand Island pile dike system and conducted clockwise circulations for 2–3 hours. Eulerian water temperature and salinity depend on many variables, including the semi-diurnal tides, neap-spring cycle, season, ocean upwelling and down welling, river discharge and bathymetry. Baker Bay served as a source of contrasting water characteristics to the main channel, injecting pockets of warmer water adjacent to Sand Island following neap higher high tides during a period of high river discharge. Velocity profiles at Baker Bay, Baker Inlet, between the Sand Island pile dikes and in the main channel were analyzed to determine the degree of logarithmic behavior at each location. Unique velocity perturbations occurred in the vicinity of the pile dikes, including reversed (upriver) flow between the pile dikes during maximum ebb.

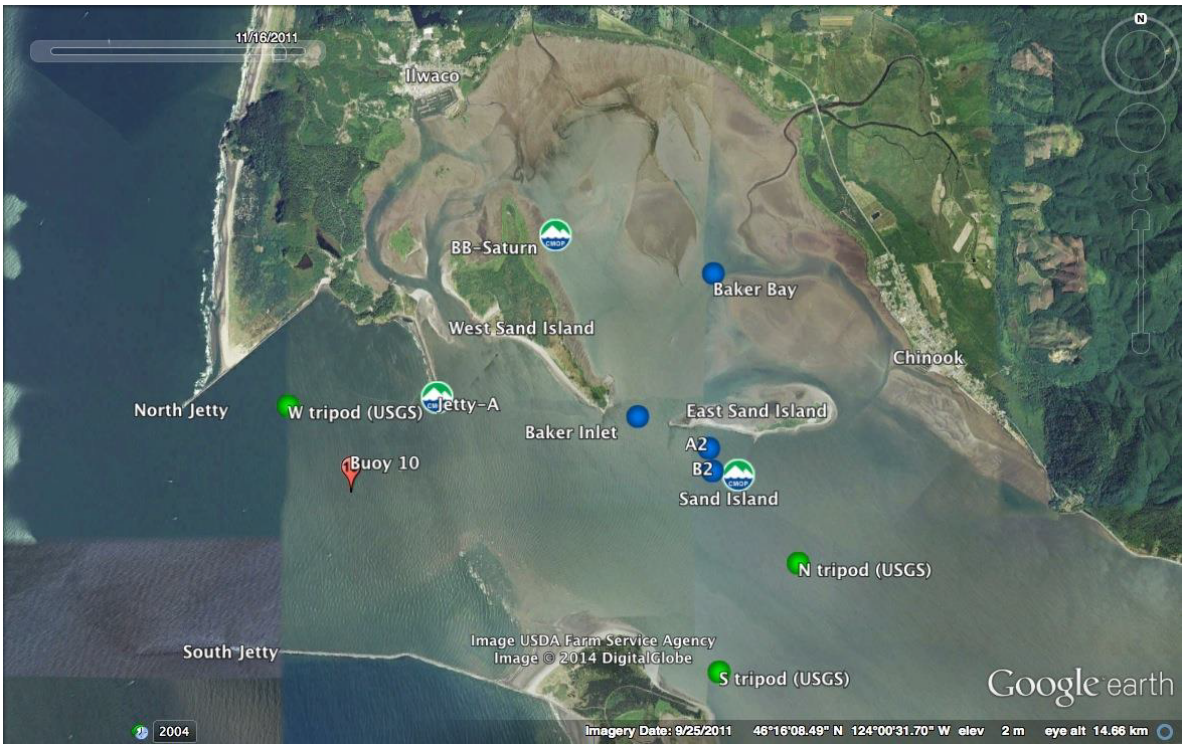

Figure 5. Google Earth image of the MCR. Blue circles indicate NPS surface-catamaran locations, green circles indicate USGS bottom-mounted tripod locations and green/white/blue logos indicate SATURN locations.

In general, the water inside Baker Bay remains fresh with transient periods of brackishness. Pure ocean water never reaches the inner parts of the bay where the two Baker Bay sensors were located. Water near the tidal flats of the northern part of Baker Bay was warmer during the data collection period due to solar insolation; this warm, fresh water was most evident during the neap tide ebb at the NPS Baker Bay sensor. Due to the location of the sensors in Baker Bay, ocean influence was indirect, as evidenced by the observed timing of temperature and salinity changes at the sensors. Temperature and salinity shifted to a more ocean-influenced regime at low tide, not at high tide as would be expected if the pathway for ocean-influenced water were direct. It is hypothesized that small amounts of ocean water enter the bay through the western (Ilwaco) and eastern (Chinook) openings during flood conditions, mix with fresher Baker Bay water, and sweep by the sensors as cooler

brackish water during ebb conditions. Water level and temperature cross-correlations at the SATURN Baker Bay sensor reinforce this indirect ocean influence concept. However, during neap tide in conjunction with higher-than normal river discharge conditions, ocean-influenced water could not always reach the Baker Bay sensors.

Examining a two-day running correlation between water level and high-pass temperature in Baker Bay allowed diagnosis of ocean influence in Baker Bay and how it changed seasonally and with the neap-spring cycle. First, the two-day running correlation was determined for the SATURN Jetty-A sensor (Figure 6, top), which represented conditions in the main river channel mid-way down the water column. A two-day window and 6-minute time step provided the best resolution of the neap-spring cycle's influence on correlation trends. At Jetty-A, small perturbations in the correlation were induced by the neap-spring cycle, but generally, the correlation was strongly positive (near +1) when ocean temperatures were warmer than river temperatures (YD 1–88 and 323–365, Figure 6, top). Rising tides were responsible for increasing water temperature at the Jetty-A sensor for all tidal ranges. Conversely, the correlation was strongly negative (near −1) when ocean temperatures were colder than river temperatures (YD 88–323, Figure 6, top). Rising tides resulted in decreasing water temperature at the Jetty-A sensor for all tidal ranges. The closer the ocean and river temperatures were to each other, the more "unstable" the correlation. The near-zero correlations around YD 101 and YD 281 may be explained by river and ocean temperatures being roughly equal at those times. YD 101 also marked the first peak in the magnitude of river discharge for the season (Figure 6, bottom).

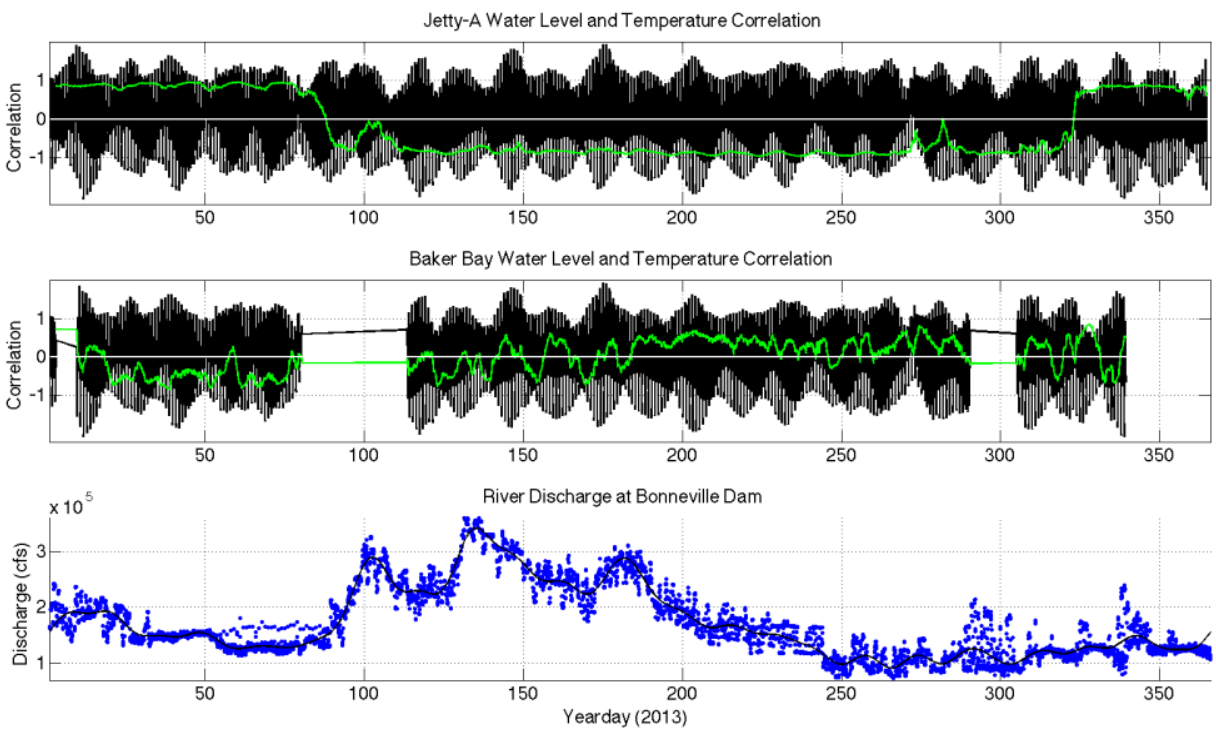

Figure 6. 2013 SATURN Jetty-A (top) and Baker Bay (middle) water level (black line) and 2-day running temperature-water level correlations (green line) and river discharge (blue dots) at Bonneville Dam (bottom).

During the high river discharge associated with the spring freshet period (YD 121–177), Baker Bay experienced alternating positive and negative correlations with the neap-spring cycle (Figure 6, middle). During spring tides (e.g., YD 157–163), ocean influenced water reached the Baker Bay

sensor, and the correlation was positive (Figure 6, middle), as would be expected during this warmer season. However, during neap tides (e.g., YD 150–155), the strong river discharge prevented much of the ocean-influenced water from reaching the Baker Bay sensor at all, resulting in a negative correlation (Figure 6, middle). Based on analysis of short-term neap tide water temperature and salinity trends, it is hypothesized that colder fresh water from the deeper southern part of Baker Bay is pushed northward across the sensor during flood flows, and warmer fresh water from the shallower northern Baker Bay tidal flats is pulled southward across the sensor during ebb flows, resulting in a predominantly negative correlation during high discharge neap tides.

Analysis of the USGS Tripods at the Mouth of the Columbia River

The USGS deployed three tripods for approximately 1.5 months (Figure 5). Wave statistics were computed using the bottom-mounted ADVs, which sampled pressure (p), and u, v, and w velocities at 8Hz for 22-minute bursts every hour. Sea surface elevation spectra were estimated from p using linear wave theory accounting for mean currents in the dispersion relationship. Wave direction and directional spreading were estimated using the methods outlined in Herbers et al. (1999). Sea-swell (0.04Hz<f<0.2Hz) and infragravity (0.004Hz<f<0.04Hz) root-mean-square (rms) wave height (H) were computed from the sea surface elevation spectra (Figure 7). There is a tidal modulation in the $H_{rms,ss}$ and $H_{rms,ig}$ due to the strong wave current interaction resulting in ~55% reduction amplitude between ebbing and flooding conditions. There is an 83% reduction in $H_{rms,ss}$ between the west and north tripod. The directional spreading as changes as function of ebb and flood conditions (Figure 8), the directional spreading is reduced during ebb flows that oppose the incoming sea-swell waves.

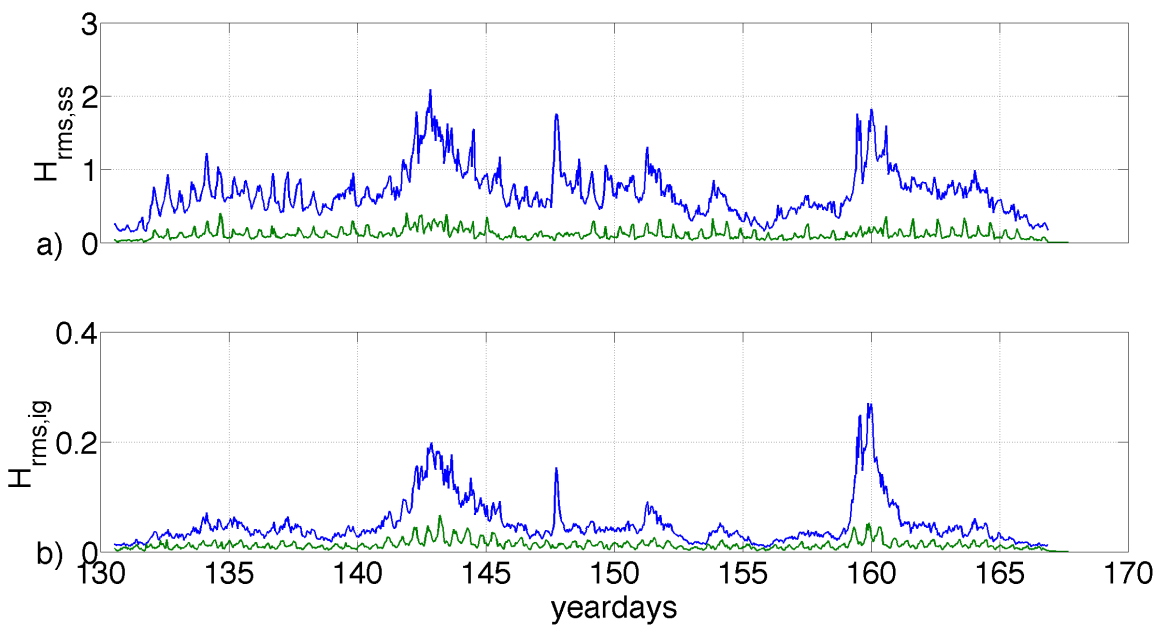

Figure 7 a) $H_{rms,ss}$ and b) $H_{rms,ig}$ for the west (blue line) and north (green line) USGS tripods.

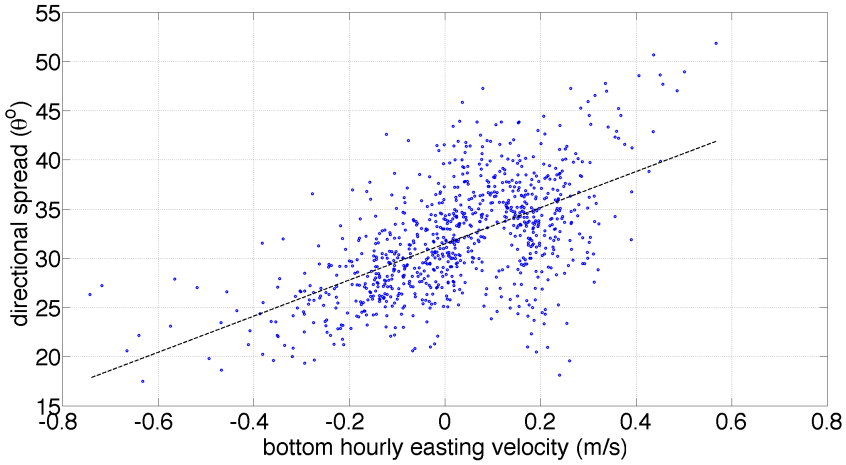

Figure 8. Directional sea-swell spreading as function of ADV time-averaged easting velocity at the USGS west tripod. Black dashed line represents linear best-fit line.

In addition, velocity data over the vertical were evaluated using ADCP data. The velocity data are rotated into a streamwise (u) coordinate frame and hourly averaged. The absolute value vertical gradient of u is computed to quantify conditions that generate large vertical shear (du/dz). There is a tidal variation associated with du/dz for all locations (Figure 9abc). For the west tripod, du/dz is smallest during flooding conditions lower in water column (Figure 9a). Larger du/dz values are observed higher in the water column in a concentrated region, which is believed to be at the interface between ocean and river water. During ebbing conditions, the shear is larger near the surface and extends to the bottom. For the north and south tripods, the shear is largest during ebbing conditions and near the bottom (Figure 9bc). Bottom salinity measurements were also obtained at tripods (Figure 9d). The bottom salinities at the north and south tripod range from oceanic to 5psu, which is believed to represent river water. The bottom salinity for the west tripod never obtains river water. Therefore stratification is still present at low tide.

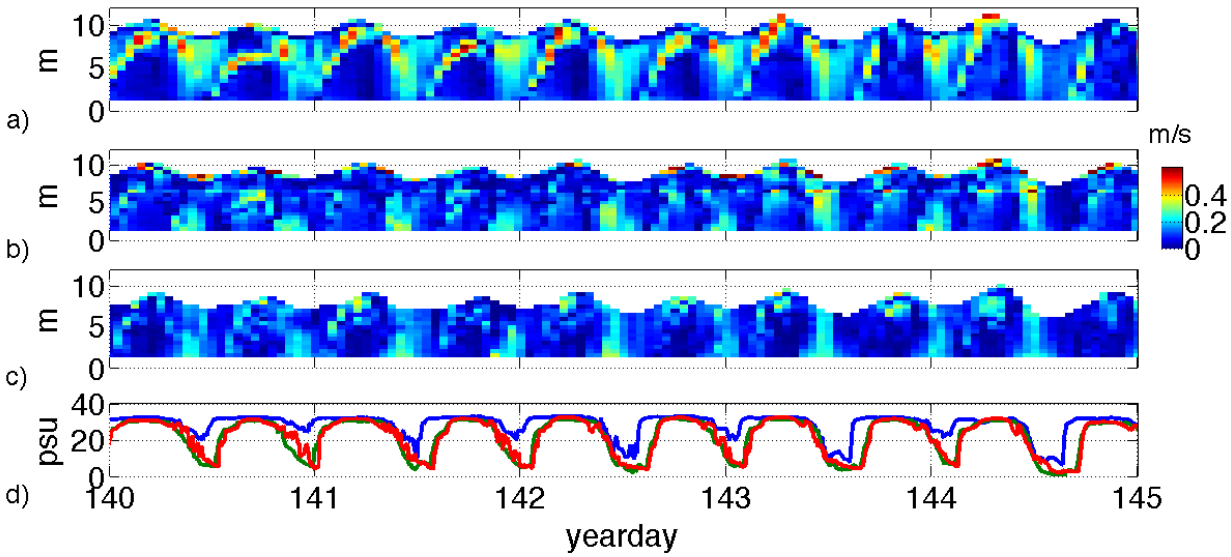

Figure 9. a) absolute values of du/dz as function time and height above the sensor for the a) west tripod, b) north tripod, c) south tripod, and d) salinity (blue line=west, green line= north, and red line=south)

Modeling of surface transport in the Mouth of the Columbia River

Drifter deployments show a wide range in trajectories depending on initial deployment conditions, i.e. time and location of release, and tidal phase. This is related to the presence of a multitude of transport mechanisms at scales ranging from wind waves to river discharge. As a result the predicted particle trajectories deviate quickly from the observations preventing a successful deterministic comparison at the level of individual drifters for tidal time scales. This in itself is not unexpected in a complex system like the Mouth of the Columbia River. However, by considering many drifters instead, the statistical confidence increases and the underlying transport patterns can be elucidated. For instance, the collection of drifters along a line may indicate the presence of a convergence zone where different water bodies meet. These convergence zones can be calculated from the model predicted surface velocity fields using the technique of Lagrangian Coherent Structures (LCS).

This analysis is performed for June 6 when a large number of GPS drifters were deployed in between the jetties just prior to a flooding tide. The corresponding model predictions were used to calculate the Finite Time Lyaponov Exponent (Reniers et al., 2010) using an integration interval of 1 hour. The ridges in the FTLE field then show the underlying LCSs that control the particle surface transport. Model calculations include the effects of waves, tides, salinity and river discharge. The model setup is similar to Elias et al. (2012) with updated boundary conditions and bathymetry.

The drifters were deployed in a grid like fashion during slack starting at the riverside of the inlet proceeding offshore. Even though the deployment was performed at high vessel speed, the first drifters already moved towards into the inlet by the time the last drifters were in the water (panel a of Figure 10) even though the total deployment took less than an hour. At this time of slack water there are no clear LCSs (panel e). Three hours after the initial deployment the drifters have separated into a northern and southern track (panel b) aligning themselves with FTLE ridges (panel f) with the remaining drifters trailing the salinity front (panel f). After approximately five hours corresponding to the reversal in the tidal velocities a single ridge has formed in the middle of the inlet that acts as an attractor (panel g). This can be inferred from the drifter motions toward this ridge in the FTLE field (compare panels b and c). Once the ebb flow increases drifters converge as they move towards the exit (panels d and h).

The presence of LCSs explains some of the dynamics observed in the drifter response. At times FTLEs align themselves with the salinity fronts (panels f and g), but are also related to differences in the bathymetry, e.g. the shallow bar in between the two tidal channels within the inlet, as well as the presence of structures such as the northern and southern jetties, jetty A and the various islands. In the future we will use the model calculations to discriminate between the different contributions to the flow dynamics in the Mouth of the Columbia River.

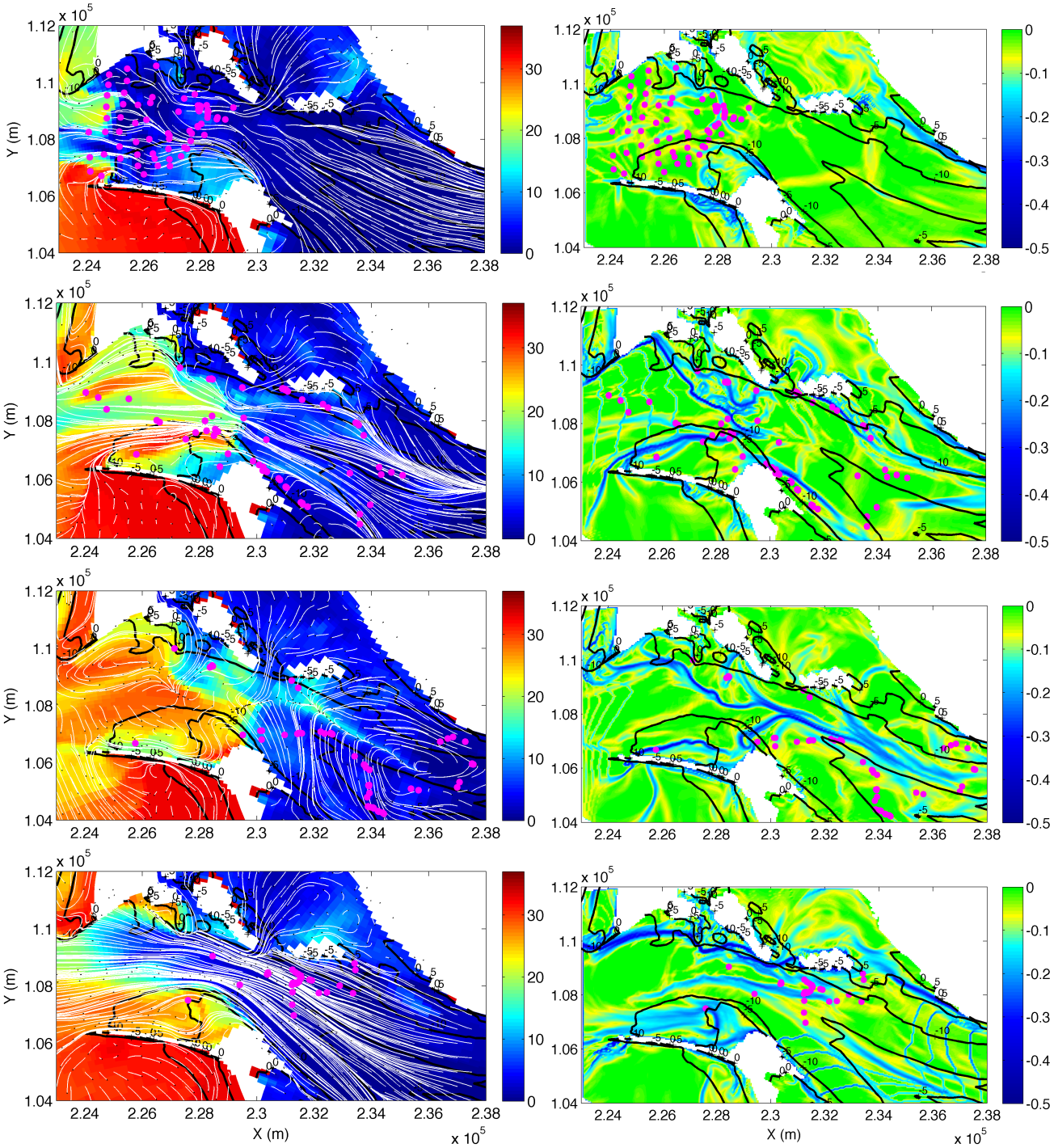

Figure 10 Left panels: Observed drifter positions (magenta), predicted flow trajectories (white arrows) and surface salinity (colors) 1, 3, 5 and 7 hours after first drifter deployment (panels a, b, c, d from top to bottom). Right panels: Observed drifter positions (magenta) and computed FTLE field 1, 3, 5 and 7 hours after first drifter deployment (panels e, f, g, h from top to bottom). Bottom contours (black) given as a reference.

Improving satellite radar surface current estimates by accounting for orbital wave motions (in collaboration with Roland Romeiser and Gordon Farquharson)

The feasibility of surface current measurements by airborne and space borne along-track interferometric (ATI) synthetic aperture radar (SAR) has been demonstrated on a number of locations. The radar measures velocity using the measured Doppler shift between the incident and reflected radiation, which includes the horizontal surface currents as well as the orbital motion of the surface waves. Therefore, a correction for the wave motion contribution has to be applied. Previously, a mean correction for the entire current field on the basis of a simple theoretical model was used. In coastal areas and river estuaries with complex current and wave patterns, this approach is not adequate because one has to account for spatial variations in the wave field and in the corresponding corrections for the current field, which can be on the same order of magnitude as the actual surface currents of interest.

To produce wave motion corrections, the numerical model Delft3D has been used to create a spatially varying wave field from which wave motion corrections can be computed. Over the course of the experiment, seven TerraSAR-X ATI images were acquired as well as a variety of collocated in-situ data sets, such as drifter trajectories and velocity profiles from ADCPs. The in-situ data has been used to validate our Delft3D model results and will also be used as a direct reference to computed velocities from the satellite radar. The model is accurately replicating the dominant processes that effect the drifter trajectories, as there is good correspondence between the virtual and actual drifters (Figure 11). Future work will be to use the wave height predictions to produce corrections for the orbital wave motions, thereby improving surface current estimates by satellite radar platforms.

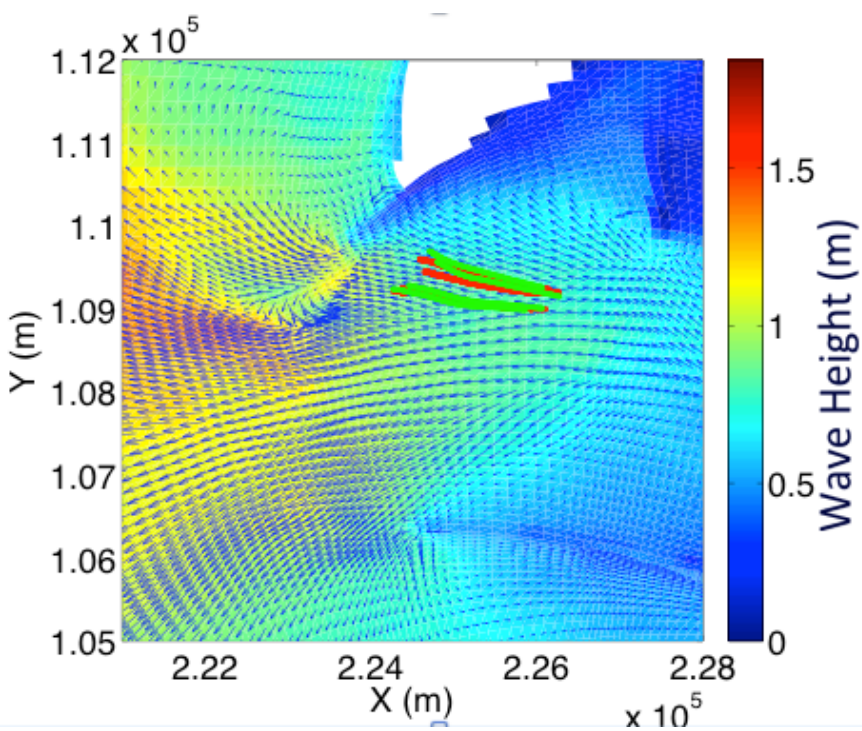

Figure 11. Plot of virtual drifters (red line) and actual drifters (green line) during the June 06 satellite overpass for a 20-minute time interval surrounding the overpass at 0200 UTC. The background color represents wave height and the vectors represent surface currents.

Tidal wave reflection and non-linearity in Elkhorn Slough, CA

The shoreward and seaward propagating tidal wave signals for a short (11km) estuary were determined using four co-located pressure and velocity sensors longitudinally deployed in Elkhorn Slough, Monterey Bay, CA to describe tidal wave reflection and distortion. Elkhorn Slough is a reflective (~100%) estuary consisting of a narrow (200m), gently sloping (1/4000) main channel with vast marshes and mud flats located along the channel. The amplitude reflection for the astronomical tidal constituents is ~90%. The amplitude reflection for tidal non-linearities, described by summing all non-astronomical tidal amplitudes, reflection is large (>125%) stating that the seaward tidal wave is more distorted than the shoreward tidal wave. It was found that the reflective time, defined as the time it takes the tidal wave to propagate to the landward boundary and back, increases as a function of tidal elevation. This is because the storage width associated with low-lying mud flats becomes more of factor in reducing the tidal phase-speed. The elevation-dependent reflective time caused by a depth-varying wave phase-speed distorts the shape of the seaward tidal wave relative to the shape of the shoreward tidal wave (Figure 12).

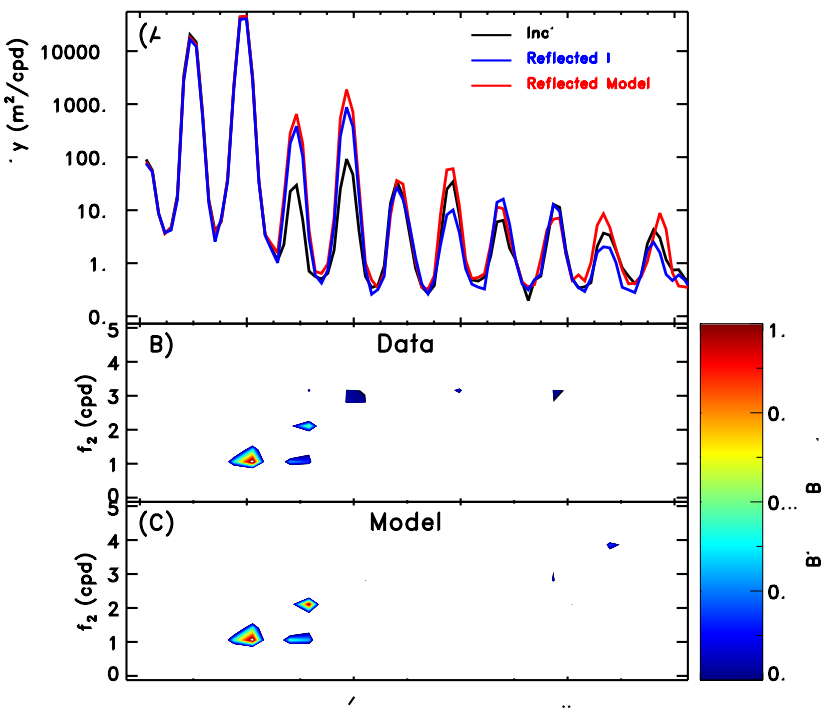

Figure 12. (A) Energy density (m^2/cpd) of observed incident (black curve), observed reflected (blue curve), and modeled reflected (red curve) waves at Elkhorn Slough (x=7.5 km) *versus* frequency (cycles per day). Contours of reflected wave bicoherence - incident wave bicoherence as a function of frequencies of the wave triads for **(B)** data and **(C)** model. The three motions in the triad are given by f_1, f_2, and (implied) $f_3=f_1+f_2$. A color scale is on the right. There are about 20 degrees of freedom in the estimates of energy density and 42 degrees of freedom in the bispectral estimates.

Low frequency seiche in a large bay (supported by ONR DURIP)

Short-term observations of sea surface elevations (η) along the 10m isobath, and long-term observations inside and outside of a large bay (Monterey Bay, CA) were obtained to describe the nodal structure of the mode 0-3 seiches within the bay and the low frequency (<346 cpd) seiche forcing mechanism. The measured nodal pattern validates previous numerical estimates associated with a northern amplitude bias, though variability exists across the modal frequency band, particularly for mode 0 and 1. Low frequency oceanic η white noise within seiche frequency bands (24-69 cpd) provides a continuous forcing of the bay seiche with a η^2 (variance) amplification of 16-40 for the different modes. The temporal variation of the oceanic η white noise is significantly correlated (R^2=0.86) at the 95% confidence interval with the bay seiche η that varies seasonally. The oceanic η white noise is hypothesized as being from low frequency, free, infragravity waves that are forced by short waves.

IMPACT/APPLICATIONS

The observations are important for understanding riverine and estuarine processes by providing high-quality data for numerical model validation. We describe the spatial variability in the CDOM-T-S relationship that are important for remote sensing. A new method for calculating inlet exchange was developed using Deflt3D. Lagrangian Coherent Structures estimated using Deflt3D model highlight the transport barriers that dynamically evolve over a tidal cycle and are compared with GPS-equipped surface drifters. Model predicted wave fields can be used to improve SAR-inferred surface velocity fields. The flow circulation within Baker Bay varies on a spring-neap cycle and is dependent on river discharge. This circulation influences the exchange of T-S with main channel of the lower Columbia River. The tidal evolution in a slough is explained using field observations and time-dependent wave reflection model for a sloping bottom.

PUBLICATIONS (2013-2014) acknowledging ONR support

Brown*, J.A., J. MacMahan, A. Reniers, E. Thornton, A.L. Shanks, S.G. Morgan, and E. Gallagher, (2014) Mass Transport on a Steep Beach*, in revision for Continental Shelf Research.*

Thornton, E.B., J. MacMahan , C. Gon, A. Reniers, S. Elgar (2014) Tidal wave reflection and distortion is Elkhorn Slough, CA., *in revision to J. of Geophys. Res.*

Brown*, J.A., J. MacMahan, A. Reniers, E. Thornton (2014) Field observations of surfzone-inner shelf exchange on a rip channeled beach, *submitted to J. Physical Oceanography.*

MacMahan. J. (2014) Low frequency seiche in a Large Bay. *submitted to J. of Physical Oceanography.*

Swick* W., J. MacMahan, A. Reniers, Thornton (2014) Observations and modeling of transverse mixing in a natural gravel-bed river, *submitted to Water Resources Research.*

Rynne, P.F., A. Reniers, J. Van de Kreeke, J. MacMahan (2014) The Effect of Tidal Exchange on Residence Time, *in preparation for Estuarine, Coasts, and Shelf Sciences.*

Ortiz-Suslow, D.G., B.K. Haus, N.J. Williams, N.M. Laxague, A.J.H.M. Reniers and H.C. Graber, 2014: The spatial-temporal variability of air-sea momentum fluxes directly measured at a tidal inlet, submitted to *J. Geophysical Res*.

Cited References

Bowers, D.G., G.E.L Harker, P.S.D Smith, P. Tett (2000) Optical properties of a region of freshwater influence (The Clyde Sea). Estuarine, Coastal, and Shelf Science, 50, 717-726.

Bowers, D.G. and H.L. Brett (2008) The relationship between CDOM and salinity in estuaries: An analytical and graphical solution, *Journal of Marine Systems* doi: 10.1016/j.jmarsys.2007.07.001.

Bowers, D.G., D. Evans, D.n. Thomas, K. Ellis, P.K le B. Williams (2004) Interpreting the coulor of an estuary, *Estuarine, Coastal and Shelf Science*, doi: 10.1016/j.ecss.2003.06.001

Chadwick, D. B., J. L. Largier. 1999. Tidal exchange at the bay-ocean boundary. Journal of Geophysical Research, Vol. 104. C12, pp. 29,901-29,924.

Elias, E., Gelfenbaum, G., and A. Van der Westhuysen. 2012. Validation of a coupled wave-flow model in a high-energy setting: The mouth of the Columbia River, Journal of Geophysical Research, 117, 21 pp.

Fischer, H.B., E.J. List, R.C.Y. Koh, J. Imberger, and N.H. Brooks. 1979. The dynamics of the vertical Mixing in Inland and Coastal Waters, 483 pp

Hojerslev, N. K., 1988: Natural occurrences and optical side effects of Gelbstoff. Report no. 50, 30pp. Institute of Physical Oceanography, University of Copenhagen.

Mehta, A. J, P. B. Joshi. 1988. Tidal Inlet Hydraulics, J. Hyrdaul. Eng., Vol. 114, No. 11, pp 1321-1338.

Nieke, B., R. Reuter, R. Heuermann, H. Wang, M. Babins, and J. C. Therriault, 1997: Light absorption and fluorescence properties of chromophoric dissolved organic matter (CDOM), in the St. Lawrence Estuary (Case 2 waters). Continental Shelf Research, 17, No.3, 235–252.

Palacios, S. L., T. D. Peterson, and R. M. Kudela, 2012: Optical characterization of water masses within the Columbia River Plume. Journal of Geophysical Research, 117, C11020, doi:10.1029/2012JC008005.

Reniers, A.J.H.M., J.H. MacMahan, F.J. Beron-Vera and M.J. Olascoaga, Rip-current pulses tied to Lagrangian coherent structures, Geophysical Res. Letters, doi:10.1029/2009GL041443, 2010.

Signell, R. P, B. Butman, 1992. Modeling tidal exchange and dispersion in Boston harbor, J. Geophys. Res., 97, NO. C10, pp 15,591 - 15,606

Smart J. H., 2004: How accurately can we predict optical clarity in the littorals. John Hopkins APL Tech. Dig., 25, No. 2, 112–120.

Stedmon, C. A., S. Markager, and H. Kass, 2000: Optical properties and signatures of chromophoric dissolved organic matter (CDOM) in Danish coastal waters. ECSS, 51, 267–278, doi:10.1006/ecss.2000.0645.

Stommel, H and H. G. Farmer. 1952. On the nature of estuarine circulation, pp. 54, Woods Hole Oceanographic Institute, Mass.

Van de Kreeke, J. 1983. Residence Time: Application to Small Boat Basins. *Journal of Waterway, Port, Coastal and Ocean Engineering, Vol. 109*, No. 4, pp 416-428.